Research Article Open Access

Mehdi Eshagh*

On Vening Meinesz-Moritz and flexural theories of isostasy and their comparison over Tibet Plateau

DOI 10.1515/jogs-2016-0013
Received November 14, 2016; accepted December 14, 2016

Abstract: Gravity and topographic/bathymetric data are used for gravimetric modelling of Moho discontinuity by hydrostatic or flexural theories of the isostasy. Here, two hydrostatic models, based on the Vening Meinesz-Moritz (VMM) principle, and two based on the loading theories and flexural isostasy are compared over Tibet Plateau. It is shown that the Moho models generated based on the VMM theory and flexural isostasy have very good agreements if the mean compensation depth and the mean elastic thickness are selected properly. However, the model computed based on the flexural isostasy is smoother. A more rigorous flexural model, which considers the membrane stress and curvature of the lithosphere, is used to model the Moho surface over the study area. It is shown that the difference between the Moho models, derived by considering and ignoring these parameters, is not significant. By combination of the flexural and VMM hydrostatic models new mathematical formulae for crustal gravity anomalies are provided and it is shown that the crustal gravity anomalies produced by them are also equivalent.

Keywords: elastic thickness, hydrostatic and flexural models, mean compensation depth, Tibet Plateau

1 Introduction

The Vening Meinesz-Moritz (VMM) inverse problem of isostasy (Sjöberg 2009) have been developed and applied successfully over different areas over the globe. In this theory, a mean isostatic compensation depth as well as a density contrast between the crust and mantle are considered for modelling the Moho undulation in such a way that the isostatic gravity anomaly vanishes. In other words, the differences between the attractions of the compensating masses underneath the topographic/bathymetric (TB) masses should be equal to the gravity anomaly. Isostasy of the Vening Meinesz type deals with the regional compensations of the TB loads rather than the local. However, considering only two parameters of mean compensation depth and density contrast seems to be insufficient to have the regional compensation from the hydrostatic theory of isostasy. Therefore, it is necessary to study this method further and compare it with the flexural isostasy, which has the regional compensation mechanism inherently and investigate how much the VMM and flexural models are in agreement.

The Moho interface, otherwise known as the Mohorovičić discontinuity, represents the boundary between the lowermost crust and the underlying uppermost mantle. Several hypotheses were proposed to explain the isotactic compensation mechanism for modelling this surface (Pratt 1854, Airy 1855 and Vening Meinesz 1931). Vening Meinesz (1931) presented a method to estimate the crustal thickness by considering a regional, instead of a local compensation scheme of topographic masses. Parker (1972) modified the Vening Meinesz theory and presented an iterative method for finding the Moho depth, and Oldenburg (1974) stabilised this method by adding a low-pass filtering technique. Gomes-Ortiz and Agarwal (2005) and Shin et al. (2007) generalised the Parker-Oldenburg method for 3-D gravity inversion, and Kiamehr and Gomes-Ortiz (2009) applied this method to estimate the Moho depth in Iran from the terrestrial gravimetric data and the Earth's gravity model EGM08 (Pavlis et al. 2008). Sünkel (1985) converted the Airy-Heiskanen Moho depth to the Vening Meinesz one by smoothing it further so that the global mean-squares error of differences between the disturbing and topographic-isostatic potentials are minimised. Sjöberg (1998a) used the Pratt and Airy models for studying isostatic geoid undulations. Furthermore, he studied the effect Airy-Heiskanen model to generate topographic-isostatic gravity potential, anomaly and the effect of analytical continuation in the Stokes's formula (see Sjöberg 1998b). Sjöberg (2009) reformulated the Moritz (1990) approach for solving the Fredholm integral equation of the first kind for recovering Moho depth and called it the VMM

*Corresponding Author: Mehdi Eshagh: Department of Engineering Science, University West, Trollhättan Sweden, E-mail: mehdi.eshagh@hv.se

inverse problem of isostasy. Braitenberg et al. (2000) presented an iterative inversion method to obtain the Moho variations under Tibet Plateau. Later on, Braitenberg et al. (2006) presented a crustal model for the South China Sea based on combined processing of satellite-gravity, bathymetric, sediment, crustal thicknesses and isostatic flexure models. Eshagh (2009) studied the lateral density variation effects of the crustal and topographic masses on the gravity field and steady-state ocean circulation explorer (GOCE) (ESA 1999) data, and Eshagh et al. (2016) utilised these data for a gravimetric recovery of the Moho density contrast in central Eurasia. The crustal density-contrast stripping corrections were applied systematically to the topographically-corrected gravity field by Tenzer et al. (2009, 2011). Braitenberg and Ebbing (2009) combined the gravity field and climate experience (GRACE) (Tapley et al. 2005) and terrestrial gravity data to study the crustal structure. In a simulation study, Sampietro (2011) investigated a possibility of using the GOCE data to recover the Moho depth. Sampietro and Reguzzoni (2011) applied the collocation and Fast Fourier Transform (FFT) techniques for recovering the Moho surface from the GOCE data. Eshagh (2014a) presented a simple, linear method for a direct Moho recovery from the satellite gravity-gradiometry data according to the VMM problem. Eshagh (2014b) developed this theory further and presented some integral formulae for Moho determination and applied them in Iran. Eshagh and Hussain (2015) investigated the relations between the geoid, gravity anomaly, deflection of the vertical and the Moho geometry. Eshagh and Hussain (2016) used the GOCE data to estimate the Moho depths for the Indo-Pakistan region. Eshagh (2016) has done a theoretical discussion about similarity of the Jeffery (1976) and VMM solutions.

In this study, two hydrostatic models, based on the plate and spherical isostatic mechanisms, and two flexural models, based on loading theories in the cases of considering and ignoring the membrane stress and curvature of the loads, are investigated. Mathematical models for such theories are provided in a consistent way to estimate the Moho flexure from each. Later, new mathematical models, based on combination of these theories, are provided, which relate gravity anomaly to the TB heights using the mechanical properties of the lithosphere. The models are applied and compared over Tibet Plateau.

2 Isostasy according to VMM model

The isostatic gravity anomaly (Δg^{I}) is defined by (cf. Sjöberg 2009):

$$\Delta g^{\mathrm{I}} = \Delta g - \Delta g_{\mathrm{TB}} + \Delta g_{\mathrm{C}} \tag{1a}$$

where Δg is the gravity anomaly, Δg_{TB} the topographic/bathymetric (TB) effect on Δg, and Δg_{C} is the isostatic compensation attraction. Equation (1a) is the principle equation used by Moritz (1990) and Sjöberg (2009) for recovering the Moho depth. The Moho variation according to Eq. (1a) and a plate shell compensation model is (see Appendix A for a proof):

$$\Delta T = -\frac{\Delta g}{2\pi G \Delta\rho} + \frac{\bar{\rho} H}{\Delta\rho} \text{ where } \Delta T = T - T_0 \tag{1b}$$

where T_0 is the mean compensation depth, T the Moho depth, G the gravitational constant, $\Delta\rho$ density contrast between the crust and mantle, H the TB heights and finally

$$\bar{\rho} = \begin{cases} \rho_{\mathrm{c}} & H \geq 0 \\ \rho_{\mathrm{w}} - \rho_{\mathrm{c}} & H < 0 \end{cases}, \tag{1c}$$

where ρ_{c} is the density of the topographic masses and ρ_{w} that of water. The difference between Eq. (1b) and the isostasy according to Airy-Heiskanen is the presence of Δg, which acts as a smoothing factor. Eshagh (2016) presented a more rigorous formula to consider the effect of the mean Moho depth into account in whole spectrum of Moho (see Appendix B):

$$\begin{aligned} T = & \frac{R}{3}\left[1 - \left(1 - \frac{T_0}{R}\right)^3\right]\left(1 - \frac{T_0}{R}\right)^{-1} \\ & - \frac{1}{4\pi G\Delta\rho}\sum_{n=0,\ n\neq 1}^{\infty}\left(\frac{2n+1}{n-1}\right)\left(1 - (n+2)\frac{T_0}{2R}\right)^{-1} \\ & \left(\Delta g_{\mathrm{TB},n} - \Delta g_n\right) \end{aligned} \tag{1d}$$

Δg_{n} and $\Delta g_{\mathrm{TB},n}$ are, respectively, the Laplace coefficients of gravity anomaly and the TB effect on it and R the Earth's radius. The first term on the right-hand side of Eq. (1d) is approximately equal to T_0 and by taking it to the left-hand side we obtain the following formula for Moho flexure:

$$\begin{aligned} \Delta T = & \frac{1}{4\pi G\Delta\rho}\sum_{n=0,\ n\neq 1}^{\infty}\left(\frac{2n+1}{n-1}\right)\left(1 - (n+2)\frac{T_0}{2R}\right)^{-1} \\ & \left(\Delta g_{\mathrm{TB},n} - \Delta g_n\right). \end{aligned} \tag{1e}$$

The series (1e) is not convergent when n increases. This is due to the presence of T_0 in the formula. If the effect of T_0 on all frequencies is neglected by equating it to zero, the global and first-order approximate solution presented

by Sjöberg (2009) will be obtained. This signal amplification depends on the size of T_0 and for larger values of T_0 the divergence occurs in lower degrees. Truncating the series to some low degrees can be regarded as a regularisation method to cut off the effect of this signal amplification. Obtaining smoother solution for larger T_0 is normal and meaningful as when the crust is thicker it resists more against the loads; see Eshagh (2016).

3 Simple model for flexural isostasy

As was explained, one way to get a smooth solution from the VMM model is to truncate the series to low degrees. In this case, the compensation of the TB masses will be regional rather than local, depending on the size of T_0. In formulating this problem, no mechanical properties of the lithosphere have been considered. For considering such properties, the problem should be solved differently. Here, the flexural theory of isostasy is used for estimating the Moho flexure due to the TB loads. In fact, the crust is assumed to be a thin elastic layer having the TB masses as loads on. Such a thin layer deforms under the pressure of the loads and the layer will be flexed under the pressure. Such a flexure follows the following partial differential equation (see Watts 2001, Stuewe 2007, p. 176, Artemieva 2011. p. 554):

$$\frac{D}{R^4}\nabla^4\Delta T + \Delta\rho\Delta T g = \bar{\rho}Hg \tag{2a}$$

where ∇^2 is the Laplacian operator, g stands for gravity, D is the rigidity of the crust:

$$D = \frac{ET_e^3}{12\left(1-\nu^2\right)} \tag{2b}$$

and E stands for the Young modulus, ν the Poisson ratio and T_e the elastic thickness of the crust. In most of literature, Eq. (2a) has been solved in the Fourier domain, but here its solution in terms of spherical harmonic is presented. We use the following spherical harmonic series for the Moho flexure (ΔT) and density-TB heights ($\bar{\rho}H$):

$$\Delta T = \sum_{n=0}^{\infty}\sum_{m=-n}^{n}(\Delta T)_{nm}\,Y_{nm}(\theta,\lambda) = \sum_{n=0}^{\infty}(\Delta T)_n \tag{2c}$$

$$\bar{\rho}H = \sum_{n=0}^{\infty}\sum_{m=-n}^{n}(\bar{\rho}H)_{nm}\,Y_{nm}(\theta,\lambda) = \sum_{n=0}^{\infty}(\bar{\rho}H)_n \tag{2d}$$

where $Y_{nm}(\theta,\lambda)$ is the fully-normalised spherical harmonic functions of degree n and order m. θ and λ are, respectively, the co-latitude and longitude, $(\Delta T)_{nm}$ and $(\bar{\rho}H)_{nm}$ are spherical harmonic coefficients of ΔT and $\bar{\rho}H$.

We know that (Turcotte et al. 1981):

$$\nabla^2 Y_{nm}(\theta,\lambda) = -n(n+1)\,Y_{nm}(\theta,\lambda) = -\kappa_n Y_{nm}(\theta,\lambda). \tag{2e}$$

Substituting Eqs. (2c) and (2d) into Eq. (2a) and writing the results in terms of the spherical harmonics yield:

$$\begin{aligned}&\frac{D}{R^4}\nabla^4\sum_{n=0}^{\infty}\sum_{m=-n}^{n}(\Delta T)_{nm}\,Y_{nm}(\theta,\lambda)\\&+g\Delta\rho\sum_{n=0}^{\infty}\sum_{m=-n}^{n}(\Delta T)_{nm}\,Y_{nm}(\theta,\lambda)\\&=g\sum_{n=0}^{\infty}\sum_{m=-n}^{n}(\bar{\rho}H)_{nm}\,Y_{nm}(\theta,\lambda)\end{aligned} \tag{2f}$$

According to Eqs. (2e) and (2f) it will not be difficult to show that the solution of the partial differential equation (2a) in spectral domain is:

$$\frac{D}{R^4}n^2(n+1)^2(\Delta T)_n + \Delta\rho g(\Delta T)_n = g(\bar{\rho}H)_n. \tag{2g}$$

After solving Eq. (2g) for ΔT_n and taking summation from both hand sides of the result, we obtain:

$$\Delta T = \sum_{n=0}^{\infty}C_n(\bar{\rho}H)_n \tag{2h}$$

where

$$C_n = \left(\kappa_n^2\frac{D}{R^4 g} + \Delta\rho\right)^{-1} \text{ and } \kappa_n^2 = n^2(n+1)^2 \tag{2i}$$

In Eqs. (2h) and (2i), when $D = 0$, then the mathematical model will be the same with the isostatic model according to Airy-Heiskanen principle. For $D > 0$, it is observed that the coefficients κ_n^2 increases so as n. The presence of $\kappa_n^2 D/(gR^4)$ in the denominator of the Moho flexure formula plays a role of regularisation factor depending on the frequency n. When D is small the ratio $D/(gR^4)$ becomes small and reduces the value of κ_n^2 and since it appears in the denominator of the solution the solution will be closer to the Airy-Heiskanen one. However, for a large value of D,the nominator will be larger and makes the solution smoother.

4 Flexural model considering membrane stress

The partial differential equation of flexure for a thin elastic spherical shell was given by Kraus (1967). Turcotte et

al. (1981) has solved this equation for studying the membrane stress in Mars and Moon. Here, we consider a simplified version of their equation. They mentioned that for the loads having much lower wavelength than the radius of the Earth, the geoid displacement due to the load is negligible. In this case, their partial differential equation changes to:

$$\left[\frac{D}{R^4}\left(\nabla^6+4\nabla^4\right)+\frac{ET_e}{R^2}\left(\nabla^2+2\right)\right]\Delta T + \left(\nabla^2+1-\nu\right)\Delta T\Delta\rho g=\left(\nabla^2+1-\nu\right)(\bar{\rho}H)\,g \qquad (3a)$$

The solution of this differential equation using spherical harmonics, according to Eqs. (2c) and (2d), considering the property (2e), is:

$$\left[\frac{D}{R^4}\left(\kappa_n^3+4\kappa_n^2\right)+\frac{ET_e}{R^2}\left(\kappa_n^2+2\right)\right](\Delta T)_n + (\kappa_n+1-\nu)\,(\Delta T)_n\,\Delta\rho g=(\kappa_n+1-\nu)\,(\bar{\rho}H)_n\,g \qquad (3b)$$

Solving Eq. (3b) for $(\Delta T)_n$ yields a similar mathematical model to the one presented in Eq. (2h), but the compensation degree C_n will be:

$$C_n=\frac{\kappa_n-(1-\nu)}{\left(\kappa_n^3-4\kappa_n^2\right)\frac{D}{R^4}+\frac{ET_e}{R^2}(\kappa_n-2)+(\kappa_n-(1-\nu))\,\Delta\rho}. \qquad (3c)$$

The membrane stress is due to the fact that the curvature of any plate drifting north-south must change to conform the curvature of the geoid (Engelder 1993, p. 383). Turcotte et al. (1981) mentioned that for the loads whose wavelengths are of the order of radius of the Earth the upwards displacement of the geoid due to the load is important. For smaller loads the contribution of the geoid and its curvature can be negligible. Figure 1 shows the plot of the compensation degree C_n computed based on Eq. (2i) and Eq. (3c). Here, an elastic thickness of 28 km and a density contrast of $\Delta\rho = 500$ kgm^{-3} are considered for the computations. The plot shows that in such conditions, the compensation degrees differ in low degrees, say up to degree 60, and they coincide after. This means that role of the curvatures is important only for low degrees. Later, our numerical studies will show how much these differences influence the Moho flexure and gravity anomaly generated from these isostasy theories.

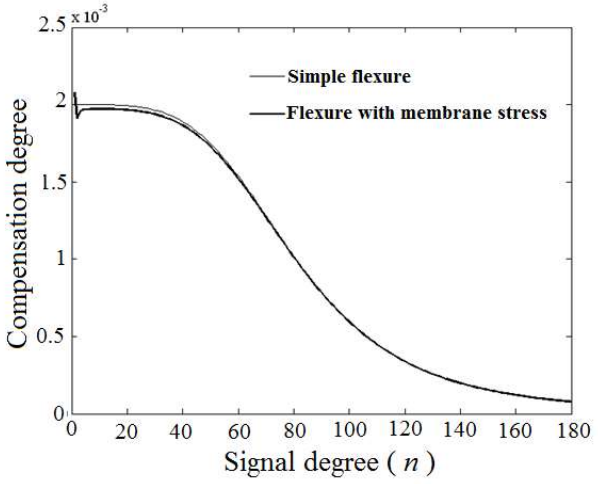

Figure 1: Compensation degree C_n according to simple flexure model, Eq. (2i) and flexure model considering membrane stress, Eq. (3c). T_0 = 33 km and T_e = 28 km.

5 Combination of VMM and flexural isostasy models

By assuming that the VMM Moho variation is the same with the Moho flexure obtained from the partial differential equation of flexure, new mathematical models can be established connecting gravity anomaly and other isostatic and mechanical properties of the lithosphere. In the case of considering the effect of crustal crystalline rocks, sediments and laterally-variable density contrast, the mantle anomalies can be computed by subtracting the computed gravity anomalies from the crustal gravity anomalies. In this case, the density and structural inhomonegnities in the mantle can be studied (Artemieva 2011, p. 554). Such a study requires a good crustal model so that the differences between the observed and computed anomalies are purely due to the mantle.

Here, the two VMM models, presented in Eqs. (1b) and (1e) are, respectively, combined with each presented flexural model by assuming that the flexures derived from all of them are equal. To begin the derivations, Eq. (1b) and Eq. (2h) are combined:

$$\sum_{n=0}^{\infty}C_n\,(\bar{\rho}H)_n=-\frac{\Delta g}{2\pi G\Delta\rho}+\frac{\bar{\rho}H}{\Delta\rho}. \qquad (4a)$$

Solving Eq. (4a) for Δg yields:

$$\Delta g=-2\pi G\left[\Delta\rho\sum_{n=0}^{\infty}(\bar{\rho}H)_n\,C_n-\bar{\rho}H\right]. \qquad (4b)$$

In order to find a more complete formula, Eq. (1e), the VMM solution is combined with the one based on the flexure theory. Eq. (1e) is solved for Δg_n

$$\Delta g_n=\Delta g_{\mathrm{TB},n}-\left(1-(n+2)\frac{T_0}{2R}\right)\left(\frac{n-1}{2n+1}\right)4\pi G\Delta\rho\,(\Delta T)_n. \qquad (4c)$$

Deriving the spectra $(\Delta T)_n$ from Eq. (2h), substituting it into Eq. (4c) and taking the summation from both sides

yield:

$$\Delta g = \Delta g_{\mathrm{TB}} - 4\pi G \sum_{n=0}^{\infty} \left(1 - (n+2)\,\frac{T_0}{2R}\right)\left(\frac{n-1}{2n+1}\right) C_n\,(\bar{\rho}H)_n. \tag{4d}$$

The VMM models (1b) and (1e) can also be combined with the flexure model (2h) and the compensation degree C_n, Eq. (3c). In this case, the mathematical models between the gravity anomaly and the TB loads are very similar to those presented in Eq. (4a) and Eq. (4d) and the only difference is the use the compensation degree C_n of Eq. (3c) instead of that presented in Eq. (2i). Therefore, these equations are not repeated to shorten the paper.

One point that should be stated here is that such mathematical models are valid for strictly one-plate planets like Mars and Moon. For the Earth, since there are toroidal flows in the mantle (Sleep and Philips 1983) and subduction zone and tectonic boundaries this mathematical model does not hold. Turcotte et al. (1981) performed similar modelling in spherical harmonic domain and thereafter they used the isostatic theory of Jeffrey (1976) for combing the flexure and isostasy models. However, our models have the following differences with respect to the solution of Turcotte et al. (1981).

- The use of VMM instead of Jeffrey's model.
- The presence of $n - 1$ in the nominator instead of $n + 1$. As the in the spherical harmonic domain $n - 1$ is involved for the gravity anomaly and $n + 1$ for the gravity disturbance; see also Sjöberg (2013).
- Jeffrey used a simple Bouguer correction for considering the topographic effect, but in Eq. (4d) a complete TB correction can be considered.

Using Eq. (4d) for prediction of gravity anomaly from the mechanical properties of the lithosphere as well as isostatic theories should give better results than the former methods.

Eshagh (2016) investigated the Jeffery and Sjöberg methods theoretically and mentioned that the Sjöberg solution is slightly better. However, a complete topographic correction has been considered in both cases. He concluded that the spectra of the computed Moho models based on these principles differ about 3 km. Eshagh et al. (2017) has estimated this difference about 3 km over the territory of Iran and mentioned that Sjöberg principle gives smoother Moho model than the Jeffrey one.

6 Flexural convolution in spherical domain

The admittance and coherent approaches (Watts 2001) are commonly used for estimation of the rigidity and elastic thickness of the crust. In this method, an approximate formula is used to find a direct mathematical relationship between the gravity anomaly and the Moho flexure. According to Braitenberg et al. (2002) the classical methods have two problems:

- averaging process over the entire grid for spectral estimation
- singularity of the ratio of the spectral of topography and gravity

Braitenberg et al. (2002) presented the flexure convolution analysis method for estimating the flexural rigidity and elastic thickness. Their idea is to perform the computations in the spatial domain rather than the spectral. In fact, they mean that for each gravity anomaly value several convolutions should be generated with different elastic thicknesses and the one, which generates closest gravity anomaly to the real one is selected as the best value for the thickness. However, they performed the computations based on the Moho flexure model that they had already computed from the gravimetric approach. In this section, we generalise their method to spherical domain using spherical harmonics and present spherical convolution for the same purpose. Also, a complete mathematical model between the gravity anomaly and flexure model is presented based on the VMM theory.

According to Heiskanen and Moritz (1967, p. 30) the Laplace coefficients $(\bar{\rho}H)_n$ can be written in terms of the Legendre polynomials and integral formula:

$$(\bar{\rho}H)_n = \frac{2n+1}{4\pi} \iint_{\sigma} \bar{\rho} H P_n(\cos\psi)\, d\sigma \tag{5a}$$

where σ is the unit sphere and $\mathrm{d}\sigma$ the surface integration element. $P_n(\cos\psi)$ stands for the Legendre polynomial of degree n with the argument ψ, which is the spherical geocentric angle between computation and integration points.

Substituting Eq. (5a) into Eq. (4d) and further simplifications yield:

$$\Delta g = \Delta g_{\mathrm{TB}} - G \iint_{\sigma} K(T_e, T_0, \psi)\, \bar{\rho} H d\sigma \tag{5b}$$

and

$$K(T_e, T_0, \psi) = \sum_{n=0}^{\infty} \left(1 - (n+2)\frac{T_0}{2R}\right)(n-1)\, C_n P_n(\cos\psi). \tag{5c}$$

No closed-form formula can be written for the kernel (5c) due to involvement of C_n. Note that C_n is a function of the elastic thickness T_e. Turcotte and Schubert (2014, p. 252) have mentioned that the loads with the wavelengths smaller than 100 km are not compensated by the lithospheric thickness. In spherical harmonic domain such a wavelength is equivalent to degree and order 180. Therefore, such a degree should be enough for calculating the kernel (5c).

Figure 2 shows the behaviour of the kernel (5c) to a geocentric angle of 10° for three values of 10, 30 and 50 km for elastic thickness (T_e) and T_0 = 33 km. The kernels are generated to degree 180 and they are all well-behaving and decay to zero after a geocentric angle of about 5°. As observed, when T_e = 10 km the kernel has its largest value in vicinity of the computation point, ψ = 0° and it is larger than the cases of T_e = 30 km and T_e = 50 km. This means that the convolution integral (5b) delivers smoother solutions for the larger values of T_e than the smaller T_e. This is quite logical and meaningful as a thicker elastic shell resists more against loads and filters out higher frequencies of solution.

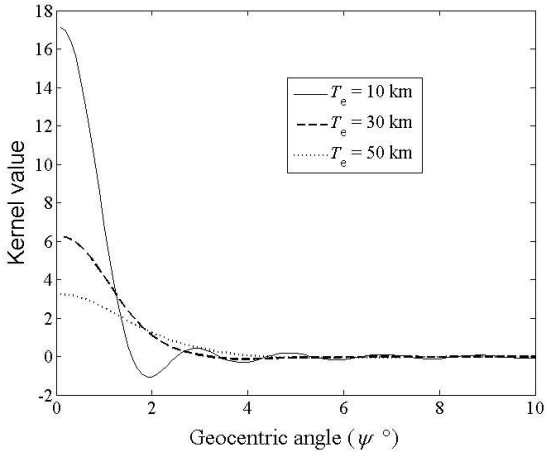

Figure 2: Kernel of convolution integral for different elastic thicknesses and T_0 = 33 km.

7 Numerical investigations

In this section, some parts of the presented theories are demonstrated numerically over a well-known area containing a large mountainous load, Tibet Plateau, where the differences between the presented theories are more visible. The reader is referred to Tenzer and Chen (2014) for a case study over this area. The studies are performed in two cases of comparing the Moho flexure models derived from the flexure theories and the hydrostatic theory of VMM as well as the seismic Moho model of CRUST1.0 (Laske et al. 2013), and generation of gravity anomalies using combination of VMM and flexure theories. It is emphasised that the goal is to compare the theories in the same conditions, rather than modelling a Moho for the area and performing geophysical interpretations.

7.1 Area and data

The study area is limited between the latitudes 20°N and 50°N and the longitudes 60°E and 110°E. The EGM08 (Pavlis et al. 2012) gravity model and the SRTM (Farr et al. 2007) TB model are used in our computations. The SRTM model contains spherical harmonic coefficients of the TB heights to degree and order 2160 and EGM08 those of the Earth's gravitational potential and partially to higher. However, according to Turcotte and Schubert (2014, p. 252) the loads having shorter wavelengths than 100 km are not compensated and therefore we use the SRTM and EGM08 models to degree and order 180.

The Moho model of CRUST1.0 are used for our comparisons. In addition, the densities and thickness of the crustal crystalline layers and densities of the upper mantle are used to compute a laterally-variable density contrast model over the study area. Furthermore, the density of the topographic masses is considered constant and equal to 2670 kgm^{-3} and the density of water 1000 kgm^{-3}.

Figure 3a represents the smooth TB heights over the study area generated from SRTM model to degree and order 180 with the maximum, mean, minimum and standard deviation 5.5, 1.5, −3.7 and 1.7 km, respectively. Truncating the spherical harmonic series causes that the positive and high values of the TB heights are seen in the central part of the area, which can somehow give an impression about the Moho deepening regime of the region.

Figure 3b is the map of gravity anomalies generated from EGM08 (Δg^{EGM08}) to the same degree. Negative values are clear over the orogenic belt of Himalayan mountain chain and are immediately followed by high positive

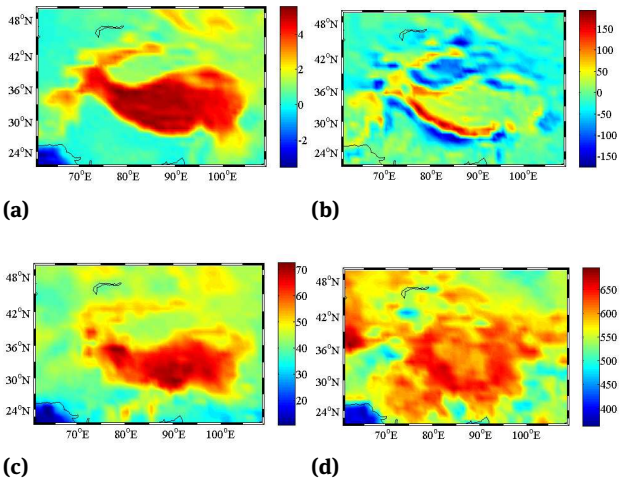

Figure 3: a) TB heights [km], b) Δg^{EGM08} [mGal], c) Seismic Moho model of CRUST1.0 [km] and d) laterally-variable density contrast derived from CRUST1.0 [kgm^{-3}].

values along the mountains and in the northern part of the area in addition to the south of Tarim Basin. Negative values have surrounded this basin except from the eastern part. Statistics of Δg^{EGM08} are given in Table 2.

Figure 3c is the map of the seismic Moho model of CRUST1.0, already limited to degree and order 180. There are similarities between this Moho model and the TB heights presented in Figure 3a, the differences can be due to the interior structure of the Earth. For example, two high values are seen in the south of the area, which are not seen in the map of TB height. These are anomalies due to the crustal crystalline density structure. In the eastern part of the area, in Afghanistan and Pakistan, no Moho deepening is visible and this could be due to the lack of seismic data over these regions. However, the map of TB heights clearly shows topographic features there. Tarim Basin is surrounded by positive values similar to what observed in Figure 3a, but the deepest parts of the Moho is visible in the west and south of Tibet Plateau rather than the centre.

Figure 3d illustrates the map of the laterally-variable density contrast $\Delta\rho$ of CRUST1.0 model. The large values are seen around the Tibet area and the lowest ones in the southwest part, over the Oman Sea and Makran Subduction zone. $\Delta\rho$ ranges from 343.9 to 694.9 kgm^{-3} over the area with the mean and STD of 566.9 and 51.4 kgm^{-3}. However, Rabbel et al. (2013) investigated some petrological and physical methods for estimating $\Delta\rho$ and concluded that $\Delta\rho$ hardly reaches to 600 kgm^{-3} over the Earth. The results of Eshagh et al. (2016) confirm their results.

7.2 Moho models based on VMM and flexural isostasy

Here, four Moho models, two based on the VMM and two based on the flexural isostasy principles are presented. The idea is to have the same mean compensation depth T_0 and elastic thickness T_e in all cases. Here and after, the Moho model computed by Eq. (1b) is named simple VMM (SVMM) and the one by Eq. (1e), VMM. The Moho model generated by the flexural model (2h) with Eq. (2i) is named simple flexure (SFLEX) and the one by Eq. (2h) and Eq. (3c) FLEX.

For Moho modelling according to the VMM theory, the choice of T_0 plays a significant role. Especially for the case where T_0 contributes to all frequencies of the solution. Here, the idea is to estimate the best value for T_0 so that the VMM Moho model has the least root mean squares error (RMS) with respect to the seismic Moho model of CRUST1.0. By trial and error a value of 33 km was estimated for T_0. This value is used for the SVMM model as well.

An important parameter in flexural isostasy is the best mean elastic thickness T_e over the study area. The FLEX model, Eq. (2h) was used and tested with different values of T_e. The FLEX model was compared to the VMM Moho model and the best T_e was found between 28 – 38 km. The RMS value of the solution does not change significantly for T_e in this interval. Karner and Watts (1983) and Jin et al. (1994) estimated an elastic thickness of 90 km over east of Himalaya, Duroy et al. (1989) reported a value of 34 km for the western part, Royden (1993) 80 km over Himalaya. Burov et al. (1990) estimated a thickness of 55 km for Tarim basin and Jin et al. (1994) a value of 40 km. However, here a larger area is considered than those selected by others and the average value of T_e should be smaller for whole region.

Figure 4 shows the maps of Moho models computed by different isostasy theories and show that they have very similar patterns. Figures 4a and 4b are the Moho maps of SVMM and VMM, respectively, and as observed, the VMM has slightly more details, in other words, the SVMM is smoother. Statistics of both models are presented in Table 1 and it is seen that the maximum and minimum of the VMM are larger than that of SVMM. The mean value of the VMM is larger by 4 km, but the maximum by 7.5 km and the minimum 1.2 km, this shows that T_0 has also contributed to all flexure spectra of Moho and not only zero-degree term of Moho depths. Figures 4c and 4d are the maps of SFLEX and FLEX, respectively and recognising their differences is not straightforward from the maps. However, what can be seen is that, these Moho models are smoother than those presented in Figures 4a and 4b. Table 1 shows their

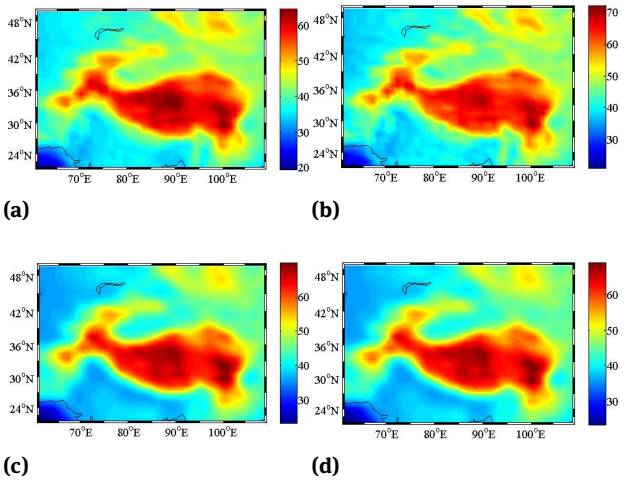

Figure 4: Maps of Moho models computed by a) SVMM, Eq. (2h), b) VMM Eq. (1e) , c) SFLEX Eq. (2h) with Eq. (2i) and d) FLEX Eqs. (2h) with Eq. (3c) [km]

statistics and illustrates that the differences are less than 1 km.

Figure 5a shows the differences between the VMM and SVMM. As can be seen the models are closer in the west of the area and most of the large differences are seen in the southeast. This is due to the significance of T_0 in all frequencies of the VMM. The models have good agreements in the Tarim basin and the southern depression of the Himalayan Mountains. Here, the same data set up to the same frequency limit were used to compute these models and the large differences can be due to the fact that spherical Earth has been considered in the mathematical modelling of VMM whilst a simple cylindrical model for the SVMM.

Figure 5b represents the differences between the SFLEX and FLEX. Generally, the models have very good agreements and their differences are less than 1 km. However, again in the eastern part of Tibet Plateau the differences are larger. No gravity anomaly was used to smooth the Moho models. However, the same TB height and density contrast models were considered as the input data in the mathematical models. Therefore, the differences are solely due to the approximations and formulation of the problem. In the FLEX model, the membrane stress and the curvature of the elastic lithosphere are taken into account. This could be a possible explanation for the larger difference in the southeast part than the rest of the area.

Figure 5c is the map of the differences between the SVMM and FLEX. Large positive values are seen over the southern depression of the Himalayan belt and the northern part of Tibet Plateau around the Tarim basin. Over Himalaya negatives values are extended to the eastern part of Tibet. Figure 5d shows a similar map to that of Figure 5c but based on the VMM. This maps shows more details, meaning that the VMM is not as smooth as the FLEX is.

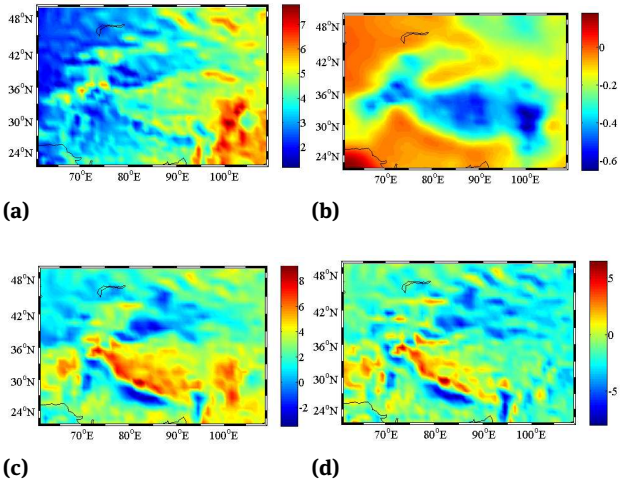

Figure 5: Maps of differences between Moho depths computed by a) VMM - SVMM, b) SFLEX and FLEX, c) SVMM – FLEX and d) VMM - FLEX [km]

Table 1 contains the statistics of the differences amongst the computed Moho models as well as the seismic Moho model of CRUST1.0. The RMS value of the differences between the SVMM and VMM is 4 km and mainly due to the difference between the mean values of these models.

The RMS of the differences between the SFLEX and FLEX models is 0.2 km, It can be concluded that considering the membrane stress and curvature of the lithosphere do not play significant roles in this area. Sleep and Philips (1983) have mentioned that the model (3a) is not suitable for the Earth due to the presence of toroidal stresses under the lithosphere. Turcotte et al. (1983) have mentioned that in the case where the load wavelength is much smaller than the radius of the Earth, Eq. (3a) can be simplified to Eq. (2a). Here, one of the largest loads on the Earth has been studied and it is seen that even for this load, the solved flexures do not significantly differ over this study area.

7.3 Generation of gravity anomaly from crustal structure

Here, the SVMM and VMM are, respectively, combined with the SFLEX and FLEX to regenerate gravity anomaly solely from the crustal structure. This can be another in-

Table 1: Statistics of different Moho models and their differences [km]

	Max	Mean	Min	STD	RMS
SVMM	64.5	43.2	19.4	8.6	–
VMM	72	47.2	20.8	9.2	–
SFLEX	69.6	45.9	22.5	9.4	–
FLEX	68.9	45.7	22.7	9.3	–
CRUST1	72.3	44.9	10.5	9.8	–
SVMM - VMM	−1.0	−4.0	−7.8	1.2	4.1
SVMM – SFLEX	3.5	−2.7	−9.1	1.8	3.2
SVMM – FLEX	3.6	−2.5	−2.5	1.7	3.0
SVMM – CRUST1.0	18.7	−1.7	−19.3	5.2	5.5
VMM – SFLEX	7.9	1.3	−6.8	1.8	2.3
VMM - FLEX	8.0	1.5	−6.4	1.8	2.3
VMM – CRUST1.0	24.9	2.2	−15.4	5.8	6.2
SFLEX – CRUST1.0	21.0	0.9	−15.9	5.7	5.8
FLEX – CRUST1.0	20.6	0.7	−16.0	5.7	5.7
SFLEX – FLEX	0.6	0.2	−0.2	0.1	0.2

dependent method of checking the theories and may be easier as the seismic data are not available with a uniform quality and good coverages. In addition, this method could be a way to predict the gravity anomalies over the areas missing gravimetric data. Subtracting such crustal gravity anomalies from the observed ones gives us some information about the density anomalies below crust.

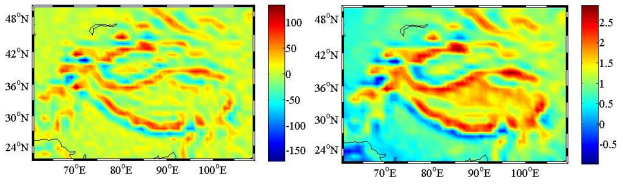

(a) (b)

Figure 6: Map of a) Δg generated from VMM and FLEX models (Δg^{VMM2}). b) Differences between $\Delta g^{\mathrm{SVMM2}}$ and Δg^{VMM2} [mGal]

Since the maps of the crustal gravity anomalies were very similar, only the one generated from the VMM and FLEX model, Eq. (4d), is presented in Figure 6a. This map is very similar to the gravity anomaly computed from EGM08, $\Delta g^{\mathrm{EGM08}}$ presented in Figure 3b. As seen, the depression in the southern part of the Himalayan Mountains chain is not pronounced so as in Figure 3b. On the other hand, the low values of this model are close to that of $\Delta g^{\mathrm{EGM08}}$, but its maximum is smaller by 60 mGal. It cannot be expected to obtain Δg in a full agreement with $\Delta g^{\mathrm{EGM08}}$ by a limited mathematical model and information. In addition, the sediments and crustal crystalline effects have not been considered in this study as the goal is to perform a comparative study between the hydrostatic VMM and flexural theories of isostasy.

Figure 6b is the map of differences between Δg generated from the combination of the SVMM and FLEX, $\Delta g^{\mathrm{SVMM2}}$, and the one computed based on the same flexural model and VMM, Δg^{VMM2}. As observed, the differences do not reach to 5 mGal over the area. The large and positive values are seen along the Himalayan Mountains and the northern parts of Tibet Plateau and Tarim basin, which already have stronger gravity.

Table 2 represents the statistics of the generated crustal gravity anomalies and their differences and it is observed that the RMS of the differences between the crustal anomalies are less than 5 mGal meaning that the presented models for the anomalies are more or less equivalent. However, the RMS of the differences between the crustal anomalies and $\Delta g^{\mathrm{EGM08}}$ is about 33 mGal for all models.

8 Conclusions

The Moho models generated based on the Vening Meinesz-Moritz theory of hydrostatic isostasy and flexural isostasy have very good agreements if the mean compensation depth and the mean elastic thickness are selected properly. Generally, the model computed based on the flexural isostasy is smoother than that based on the VMM. The simple Moho model, computed by Eq. (1b), and the one computed based on the spherical Earth, Eq. (1d), have good agreements as long as the spherical harmonic expansions, which are used for generating the topographic/bathymetric heights and gravity anomalies for both models are limited to degree and order 180. The flexural models (2h) with (2i) and (3c) produce the same Moho model even for large loads on the Earth's lithosphere. Combinations of the flexural and VMM hydrostatic model lead to new mathematical models for computing the crustal gravity anomalies. It was shown that all different way of combinations lead to more or less the same crustal gravity anomaly in the case of choosing proper mean compensation depth and elastic thickness. Considering the crustal crystalline rocks and sediments effects will further improve our crustal anomalies and subtracting them from the observed ones give the opportunity of studying subcrustal and mantle density anomalies.

Table 2: Statistics of generated gravity anomalies from the crustal models and their differences. $\Delta g^{\mathrm{SVMM1}}$ from SVMM and SFLEX, $\Delta g^{\mathrm{SVMM2}}$ SVMM and FLEX, Δg^{VMM1} VMM and SFLEX and Δg^{VMM2} VMM and FLEX. [mGal]

	Max	Mean	Min	STD	RMS
$\Delta g^{\mathrm{SVMM1}}$	138.2	0.0	−183.3	33.4	–
Δg^{VMM1}	136.4	0.0	−181.1	32.9	–
$\Delta g^{\mathrm{SVMM2}}$	144.7	3.3	−178.9	33. 8	–
Δg^{VMM2}	141.1	2.0	−178.2	33.2	–
$\Delta g^{\mathrm{EGM08}}$	192.7	−10.3	−175.4	45.3	–
$\Delta g^{\mathrm{SVMM1}} - \Delta g^{\mathrm{VMM1}}$	1.74	0.0	−2.2	0.5	0.5
$\Delta g^{\mathrm{SVMM1}} - \Delta g^{\mathrm{SVMM2}}$	3.2	−3.3	−10.1	2.6	4.2
$\Delta g^{\mathrm{SVMM1}} - \Delta g^{\mathrm{VMM2}}$	3.2	−1.9	−7.8	2.2	2.9
$\Delta g^{\mathrm{SVMM1}} - \Delta g^{\mathrm{EGM08}}$	130.1	10.3	−133.2	31.0	32.7
$\Delta g^{\mathrm{VMM1}} - \Delta g^{\mathrm{SVMM2}}$	3.2	−43.3	−10.2	2.8	4.3
$\Delta g^{\mathrm{VMM1}} - \Delta g^{\mathrm{VMM2}}$	3.1	−1.9	−7. 7	2.2	3.0
$\Delta g^{\mathrm{VMM1}} - \Delta g^{\mathrm{EGM08}}$	131.0	10.3	−134.2	31.1	32.7
$\Delta g^{\mathrm{SVMM2}} - \Delta g^{\mathrm{VMM2}}$	3.6	1.3	−1.1	0.7	1.5
$\Delta g^{\mathrm{SVMM2}} - \Delta g^{\mathrm{EGM08}}$	131.4	13.6	−126.9	29.9	32.8
$\Delta g^{\mathrm{VMM2}} - \Delta g^{\mathrm{EGM08}}$	131.2	12.3	−129.4	30.0	32.4

Appendix A: A proof for Eq. (1b)

The effect of the TB masses on gravity anomaly can be computed by a plate shell model (see e.g. Turcotte and Schubert 2014, p. 247):

$$\Delta g_{\mathrm{TB}} = 2\pi G \int_{o}^{H} \bar{\rho}\, dz \tag{A.1}$$

where G is the Newtonian gravitational constant, dz the vertical integration element. By assuming that $\bar{\rho}$ is constant radially and performing the integration of Eq. (A.1), the gravitational attraction of the TB masses becomes:

$$\Delta g_{\mathrm{TB}} = 2\pi G \bar{\rho} H. \tag{A.2}$$

Eq. (A.2) is nothing else than the Bouguer correction to gravity. Similarly, the effect of the compensation masses on gravity anomaly can be derived:

$$\Delta g_{\mathrm{C}} = 2\pi G \int_{T}^{T_0} \Delta\rho\, dz \tag{A.3}$$

where T is the Moho depth and T_0 the mean compensation depth and $\Delta\rho$ is the density contrast between the crust and upper mantle. Again by assuming that $\Delta\rho$ is constant radially and taking the integration, we have:

$$\Delta g_{\mathrm{C}} = 2\pi G \Delta\rho \left(T_0 - T\right). \tag{A.4}$$

The crust is in isostatic equilibrium according to the AH mechanism, this means that Eq. (A.2) should be equal to Eq. (A.4). By equating these equations and solving the results for T, we get:

$$T = T_0 - \frac{\bar{\rho} H}{\Delta\rho}, \tag{A.5}$$

which is nothing else than the Moho depth based on the AH mechanism; see e.g. Heiskanen and Moritz (1967, p. 135).

Also, the Moho can be computed based on the fact that the isostatic gravity anomaly (Δg^{I}) should be zero (Sjöberg 2013, Eq. 12):

$$\Delta g^{\mathrm{I}} = \Delta g - \Delta g_{\mathrm{TB}} + \Delta g_{\mathrm{C}} = 0. \tag{A.6}$$

Substituting Eqs. (A.2) and (A.4) into Eq. (A.6) and solving the result for T lead to:

$$T = T_0 + \frac{\bar{\rho} H}{\Delta\rho} - \frac{\Delta g}{2\pi G \Delta\rho}. \tag{A.7}$$

Appendix B: A proof for Eq. (1d)

Now, $\Delta\rho$, T and H are assumed to be laterally-variable and the surface integrations are performed globally rather than regionally. In this case, the TB effect on the gravity anomaly is (Eshagh and Hussain 2015):

$$\Delta g_{\mathrm{TB}} = 4\pi G \sum_{n=0}^{\infty} \frac{n-1}{2n+1} \left\{ \left(\bar{\rho} H\right)_n + \frac{n+2}{2R} \left(\bar{\rho} H^2\right)_n + \frac{(n+2)(n+1)}{6R^2} \left(\bar{\rho} H^3\right)_n \right\}. \tag{B.1}$$

Sjöberg (2009) has written the following integral formula for the compensation potential:

$$V_C = G\Delta\rho \iint_\sigma \int_{R-T}^{R-T_0} \frac{r'^2 dr'}{l} d\sigma$$
$$= G\Delta\rho \iint_\sigma \int_{R-T_0}^{R} \frac{r'^2 dr'}{l} d\sigma - G\Delta\rho \iint_\sigma \int_{R-T}^{R} \frac{r'^2 dr'}{l} d\sigma$$
$$= V_{C0} + dV_C. \quad \text{(B.2)}$$

According to the Legendre expansion of l^{-1} (Heiskanen and Moritz 1967, p. 33)

$$\frac{1}{l} = \sum_{n=0}^{\infty} \frac{r'^n}{r^{n+1}} P_n(\cos\psi) \quad \text{(B.3)}$$

and substituting it into the first integral of Eq. (B.2) and solving the integral read:

$$V_{C0} = G\Delta\rho \iint_\sigma \sum_{n=0}^{\infty} \frac{1}{r^{n+1}} \frac{1}{n+3} \int_{R-T_0}^{R} r'^{n+2} dr' P_n(\cos\psi) d\sigma$$
$$= G\Delta\rho \iint_\sigma \sum_{n=0}^{\infty} \frac{R^{n+3}}{r^{n+1}} \frac{1}{n+3} \left[1 - \left(1 - \frac{T_0}{R}\right)^{n+3}\right] P_n(\cos\psi)\, d\sigma. \quad \text{(B.4)}$$

The gravity anomaly mean attraction compensation will be (cf. Sjöberg 2013, eq. 19a):

$$\Delta g_{C0} = \frac{4\pi G R \Delta\rho}{3} \left[1 - \left(1 - \frac{T_0}{R}\right)\right]. \quad \text{(B.5)}$$

If we repeat a similar derivation for the second term of Eq. (B.2) considering that T is laterally-variable, the effect of compensation masses on gravity anomaly will be:

$$\Delta g_C = \Delta g_{C0}$$
$$- GR\Delta\rho \sum_{n=0}^{\infty} \frac{n-1}{n+3} \iint_\sigma \left[1 - \left(1 - \frac{T}{R}\right)^{n+3}\right] P_n(\cos\psi)\, d\sigma. \quad \text{(B.6)}$$

The Taylor expansion of the binomial term in Eq. (B.6) yields:

$$\left(1 - \frac{T}{R}\right)^{n+3} \approx 1 - (n+3)\frac{T}{R} + (n+3)(n+2)\frac{T^2}{2R^2}. \quad \text{(B.7)}$$

Substituting Eq. (B.7) into Eq. (B.6), assuming $T^2 \approx TT_0$ and further simplification yield:

$$\Delta g_C = \Delta g_{C0}$$
$$- GR\Delta\rho \sum_{n=0}^{\infty} (n-1)\frac{T}{R} \iint_\sigma \left(1 - (n+2)\frac{T_0}{2R}\right) P_n(\cos\psi)\, d\sigma. \quad \text{(B.8)}$$

Since T_0 is constant, it can be taken out of the integral of Eq. (B.8), and we already know according to (Heiskanen and Moritz 1967, p. 30):

$$T_n = \frac{2n+1}{4\pi} \iint_\sigma T\, P_n(\cos\psi)\, d\sigma. \quad \text{(B.9)}$$

According to Eq. (B.9), Eq. (B.8) is simplified and the spectral form of the result will be:

$$\Delta g_{C_n} = \Delta g_{C0}\delta_{n0} - 4\pi G\Delta\rho \frac{n-1}{2n+1} T_n \left(1 - (n+2)\frac{T_0}{2R}\right). \quad \text{(B.10)}$$

By considering Eq. (A.6) in the spectral form and substituting Eq. (B.5) and (B.10) into it, we obtain:

$$\Delta g_n - \Delta g_{TB,n} + \Delta g_{C0}\delta_{n0}$$
$$= 4\pi G\Delta\rho \frac{n-1}{2n+1} T_n \left(1 - (n+2)\frac{T_0}{2R}\right). \quad \text{(B.11)}$$

Solving Eq. (B.11) for T_n and taking summation from both sides of the equation yield Eq. (1d).

Acknowledgement: The authors is thankful to Professor Lars E. Sjöberg and the three reviewers for their constructive and useful comments to the manuscript.

References

Airy, G. B., 1855. On the computations of the effect of the attraction of the mountain masses as disturbing the apparent astronomical latitude of stations in geodetic surveys, Transactions Royal Society of London, 145 (B), pp. 101-104.

Artemieva I., 2011. The lithosphere, An interdisciplinary approach, Cambridge University Press.

Braitenberg, C., Ebbing, J., 2009. New insights into the basement structure of the west-Siberian basin from forward and inverse modelling of Grace satellite gravity data. Journal of Geophysical Research 114, B06402.

Braitenberg, C., Wienecke, S., Wang, Y., 2006. Basement structures from satellite-derived gravity field: South China Sea ridge, Journal of Geophysical Research 111, B05407.

Braitenberg, C., Zadro, M., Fang, J., Wang, Y., Hsu, H.T., 2000. The gravity and isostatic Moho undulations in Qinghai-Tibet plateau. Journal of Geodynamics 30 (5), pp. 489-505.

Burov, E.B., Kogan, M. G., Lyon-Caen, H., and Molnar, P., 1990. Gravity anomalies, the deep structure, and dynamic processes beneth the Tien Shan, Earth Planetary Science Letters, 96, pp. 367-383.

Duroy Y., Farah A., and Lillie R. J., 1989. Subsurface densities and lithospheric flexure of the Himalayan foreland in Pakistan, in Malinconico, L.L., and Lillie R.J. Eds, Tectonics of the western Himalaya, Special Paper 232, Geol. Soc. Am. pp. 217-236.

Engelder T., 1993. Stress regime in the lithosphere, Princeton University Press.

ESA (1999) Gravity Field and Steady-State Ocean Circulation Mission, ESA SP-1233(1), Report for mission selection of the four candidate earth explorer missions, ESA Publications Division, pp. 217, July 1999.

Eshagh, M., 2009. The effect of lateral density variations of crustal and topographic masses on GOCE gradiometric data: a study in Iran and Fennoscandia, Acta Geodaetica et Geophysica Hungarica 44 (4), pp. 399-418.

Eshagh, M., 2014a. Determination of Moho discontinuity from satellite gradiometry data: linear approach, Geodynamics, Research International Bulletin 1, 2, pp. 1–13.

Eshagh, M., 2014b. Integral development of Vening Meinesz-Moritz formula for local determination of Moho discontinuity with applications in Iran, Geodynamics, Research International Bulletin, 2, 3, I-IX.

Eshagh, M., 2016. A theoretical discussion on Vening-Meinesz-Moritz inverse problem of isostatsy, Geophysical Journal International, 207, 1420-1431.

Eshagh, M. and Hussain, M., 2015. Relationship amongst gravity gradients, deflection of vertical, Moho deflection and the stresses derived by mantle convections-a case study over Indo-Pak and surroundings, Geodynamics, Research International Bulletin, 3 (4), pp. I-XIII.

Eshagh, M., and Hussain, M., 2016. An approach to Moho discontinuity recovery from on-orbit GOCE data with application over Indo-Pak region, Tectonophysics, 690, Part B, 253-262.

Eshagh, M., Hussain, M., Tenzer, R., Romeshkani, M., 2016. Moho Density Contrast in Central Eurasia from GOCE Gravity Gradients, Remote Sensing 8, 418. pp. 1-18

Eshagh, M., Ebadi, S. and Tenzer, R., 2017. Isostatic GOCE Moho model for Iran, submitted

Farr, T. G., Paul, A. R., Edward, C., Robert, C., Riley, D., Scott, H., Michael, K., Mimi, P., Ernesto Rodriguez, Ladislav, R., David, S., Shaffer, S., Joanne, S., 2007. The Shuttle Radar Topography Mission, Reviews of Geophysics 45, RG2004.

Gomez-Oritz, D., Agarwal, B. N. P., 2005. 3DINVER.M: a MATLAB program to invert the gravity anomaly over a 3D horizontal density interface by Parker-Oldenburg's algorithm, Computers & Geosciences 31, pp. 13-520.

Heiskanen, W.A., 1931. New isostatic tables for the reduction of the gravity values calculated on the basis of Airy's hypothesis, Bulletine Grodesique, 30, pp. 110-129.

Heiskanen, W. and Moritz, H., 1967. Physical geodesy, W.H. Freeman and company, San Francisco and London.

Jeffrey, H., 1976. The earth: its origin, history and physical constitution, 6th edition, Cambridge University Press.

Jin Y., McNutt, M.K. and Zhu Y., 1994. Evidence from gravity and topography data for folding in Tibet: Nature, 371, pp. 669-674.

Karner G.D. and Watts A.B., 1983. Gravity anomalies and flexure of the lithosphere at mountain ranges, Journal of Geophysical Research, 88, pp. 10449-10477.

Kiamehr, R., Gomes-Ortiz, D., 2009. A new 3D Moho depth model for Iran based on the terrestrial gravity data and EGM2008 model. EGU General Assembly Vol. 11, EGU2009-321-1, Vienna, Austria (Abstract).

Kraus H., 1967. Thin elastic shells: an introduction to the theoretical foundation and analysis of their static and dynamic behaviour, 476 pp., John Wiley.

Laske, G., Masters, G., Ma, Z., Pasyanos, M., 2013. Update on CRUST1.0 - A 1-degree Global Model of Earth's Crust. In EGU General Assembly Conference Abstracts 15, 2658.

Moritz, H., 1990. The figure of the Earth, H Wichmann, Karlsruhe.

Oldenburg, D.W., 1974. The inversion and interpretation of gravity anomalies. Geophysics 39, pp. 526-536.

Parker, R.L., 1972. The rapid calculation of potential anomalies. Geophysical Journal of the Royal Astronomical Society 31, pp. 447-455.

Pavlis, N., Holmes, S.A., Kenyon, S.C., Factor, J.K., 2008. An Earth Gravitational model to degree 2160: EGM2008. Presented at the 2008 General Assembly of the European Geosciences Union, Vienna, Austria, April 13-18, 2008.

Pratt, J.H., 1854. On the attraction of Himalayan mountain and of the elevated regions beyond them, upon the plumb line in India, Philosophical transaction of the Royal society of London, 146, pp. 53-100.

Rabbel, W., Kaban, M., Tesauro, M., 2013. Contrasts of seismic velocity, density and strength across the Moho. Tectonophysics, 609, pp. 437–455.

Royden L., 1993. The tectonic expression of slab pull at convergent plate boundaries, Tectonics, 12, pp. 303-325.

Sampietro, D., 2011. GOCE exploitation for Moho modelling and applications. In proceedings of the 4th international GOCE user workshop, Munich, Germany, vol. 31.

Sampietro, D., Reguzzoni, M., 2011. A study on the Austrian Moho from GOCE data. Poster presented at European Geosciences Union General Assembly 2011 Vienna, Austria, 08 April 2011.

Shin, Y.H., Xu, H., Braitenberg, C., Fang, J. Wang, Y., 2007. Moho undulations beneath Tibet from GRACE-integrated gravity data. Geophysical Journal International 170, pp. 971-985.

Sjöberg, L.E., 1998a, On the Pratt and Airy models of isostatic geoid undulations. Journal of Geodynamics, 26, 1, 137-147.

Sjöberg, L.E., 1998b, The exterior Airy/Heiskanen topographic-isostatic gravity potential, anomaly and the effect of analytical continuation in Stokes's formula. Journal of Geodesy, 72, 654-662,

Sjöberg, L.E., 2009. Solving Vening Meinesz-Moritz Inverse Problem in Isostasy, Geophysical Journal International 179, pp. 1527-1536.

Sjöberg, L. E., 2013. On the isostatic gravity anomaly and disturbance and their applications to Vening Meinesz-Moritz inverse problem of isostasy, Geophysical Journal International, 193, pp. 1277–1282.

Sleep, N.H., and Phillips, R.J., 1985. Gravity and lithospheric stress on the terrestrial planets with reference to the Tharsis region of Mars, Journal of Geophysical Research. 90, B6, pp. 4469-4489.

Stuewe, K. (2007) Geodynamics of the lithosphere, Springer 2nd edition

Sünkel, H., 1985. An isostatic Earth model, Report 367, Department of Geodetic Science and Surveying, Ohio State University, Columbus. Ohio.

Tapley, B., Ries, J., Bettadpur, S., Chambers, D., Cheng, M., Condi, F., Gunter, B., Kang, Z., Nagel, P., Pastor, R., Pekker, T., Poole, S., Wang, F., 2005. GGM02-An improved Earth gravity field model from GRACE. Journal Geodesy 79, pp. 467-478.

Tenzer, R., and Chen, W., 2014. Regional gravity inversion of crustal thickness beneath the Tibetan plateau. Earth Science Informatics, 7, 4, pp. 265-276.

Tenzer, R., Hamayun, Vajda, P., 2009. Global maps of the CRUST2.0 components stripped gravity disturbance, Journal of Geophysical Research (Solid Earth) 114, B05408.

Tenzer R, Novák P, Gladkikh V., 2011. On the accuracy of the bathymetry-generated gravitational field quantities for a depth-dependent seawater density distribution. Studia Geophysica et

Geodaetica 55(4), pp. 609-626.
Turcotte, D. and Schubert, G. 2014. Geodynamics, third edition, Cambridge University Press
Turcotte, D., Willemann R.J. Haxby W.F. and Norberry J., 1981. Role of memberane stresses in the support of planetary topography, Journal of Geophysical Research, 86, pp. 3951-3959.
Vening Meinesz, F.A., 1931. Une nouvelle methode pour la reduction isostatique regionale de l'intensite de la pesanteur. Bulletine Geodesique., 29, 1, pp. 33-51.
Watts A. B., 2001. Isostasy and flexure of the lithosphere, Cambridge University Press, 458 pp.